Springer

KSME

Journal of Mechanical Science and Technology 24 (10) (2010) 2143~2150
www.springerlink.com/content/1738-494x
DOI 10.1007/s12206-010-0710-z

Geometric optimization for a thermal microfluidic chip†

Meysam Rahmat and Pascal Hubert*

Department of Mechanical Engineering, McGill University, 817 Sherbrooke St. West, Montreal, Quebec, Canada, H3A 2K6

(Manuscript Received October 30, 2009; Revised June 8, 2010; Accepted June 8, 2010)

Abstract

A geometric design for a microfluidic chip using numerical simulation is presented. Finite element method was employed in order to design the microchannel configuration for a microfluidic chip array. The effect of geometry on the thermal response at the interface between the microfluidic chips and an integrated system, such as a micro-electronic device, was investigated. Dimensionless design charts, obtained from the parametric models, demonstrated that a compromise between a maximum heat transfer and a minimum interface temperature was achieved with an equilateral triangle cross-section at a microchannel spacing to width ratio of two. The transient response of the microfluidic chip implied that the transient analysis corresponded to the steady state results under different boundary conditions.

Keywords: Finite element; Heat transfer; Microchannel; Steady state; Transient

1. Introduction

Microfluidics, fluid mechanics at the micro scale, has received more attention in the past years due to its ever-increasing applications. The adaptability of microfluidic devices, from micro heat pipes [1] in highly compacted integrated circuits to cell analysis in Bio Microelectromechanical Systems (BioMEMS) [2], has been a key factor in their wide range of applications. The main functions of microfluidic devices in microelectronics are to maintain the electronic components below a critical temperature and to increase the level of temperature uniformity. However, for BioMEMS, the extensive range of requirements calls for the development of new applications for microfluidic devices, such as small volume sampling for glucose monitoring in biosensors [3].

Various aspects of enhanced heat transfer, from heat pipes [4] to micro flow heated channels [5], have been investigated in the last decades. In microelectronics, microfluidic chips provide attractive solutions for the thermal management in highly compacted integrated circuits [6]. A significant number of investigations have been carried out on different micro fluid flow/heat transfer devices such as micro heat pipes [1], micro-fin tubes [7], micro heat sinks [8], micro loop heat pipes [9], and micro heat pipe spreaders [10]. The minimization of the heat losses in temperature sensors and heaters has been carried out by a micro-jet impingement cooling heat transfer process, and as a result a uniform heat flux along the wall has been provided [5, 11].

Recently developed manufacturing technologies have expanded the range of material choices for MEMS technologies. The development of the new generation of polymeric lab-on-a-chip devices is accelerated because of the cost effectiveness, ease of manipulation and recyclability of polymers. Particularly, the use of polymers for manufacturing microfluidic chips has several advantages including chemical inertness and stability in aqueous environments. Attaching polymeric microfluidic systems to different materials, such as glass [12], provides better optical detection for microfluidic systems for transparent polymers. Use of polymeric microfluidic chips rather than silicon wafer chips in the thermal applications has also various advantages. Most of the microfluidic chip manufacturing techniques utilize different methods of etching silicon [6] as the substrate for microchannels. However, in some applications, such as temperature sensors, having highly conductive substrates, such as silicon, leads to undesirable heat losses from the walls and non-uniform heat flux boundary conditions in the heated walls [5]. Therefore, research has been carried out to reduce the axial conductivity of the substrate in microfluidic chips [11]. New techniques for manufacturing complex microfluidic devices, such as robotic deposition of a fugitive organic ink impregnated with an epoxy resin [13], were also developed. Although epoxy has a very low thermal conductivity (around 1 *W/m°C*), even in the applications where a high effective conductivity is desirable, the possibility of making a three-dimensional microchannel configuration can significantly increase the overall thermal efficiency.

† This paper was recommended for publication in revised form by Associate Editor Ji Hwan Jeong
*Corresponding author. Tel.: +1 514 3986303, Fax: +1 514 3987365
E-mail address: pascal.hubert@mcgill.ca
© KSME & Springer 2010

Furthermore, the low conductivity of epoxy is beneficial for measuring temperature in sensor applications. For heat removal applications, the use of high conductive epoxies through the addition of conductive particles, such as silver nano particles [14], can significantly improve the thermal conductivity.

The geometric optimization of microfluidic chips has always been of interest. Although for some applications, the geometric parameters are dictated by the required patterns of the microchannels [15], research has been primarily conducted on the geometric optimization of microfluidic chips particularly for heat transfer applications. The effects of thermophysical properties and design parameters of micro heat pipe [16] and groove geometries [17] have been addressed based on capillary limits. The effect of geometry on the maximum heat transport of triangular micro heat pipes was also investigated for an array of microchannels and the results were evaluated by theoretical modelling [18]. Ma and Peterson investigated the effect of width of triangular microchannels on the maximum heat transport for ten grooved plates with identical apex angles of 60°. Peterson et al. [19] found the maximum temperature of a silicon wafer and the effective thermal conductivity of micro heat pipe arrays experimentally. They also presented the temperature gradient along the axis of the microchannels. The impact of microchannel geometry on the heat transfer in the electronic cooling application was studied by Dickey and Lam [20]. Using numerical simulation, Dickey and Lam considered an array of triangular microchannels and investigated the effect of microchannel gap distance and microchannel size on the average temperature of the top surface. Covering a range of 0–60 μm for the gap distance, they suggested the value of 6 μm independently of the microchannel size. A more detailed geometric optimization on rectangular microchannels made in silicon wafer was conducted by Li and Peterson [21]. They mainly considered the thermal resistance as the objective function and suggested 120 channels per centimeter. Single-phase flow [8] and two-phase flow [22] as different regimes in microchannels have been investigated, while phase changes in microchannels were addressed by Zhang et al. [23].

Most of the previous investigations on the geometric aspects of microchannel thermal performance dealt with a single microchannel [24–26], and provided specific suggestions for a given problem. However, the effect of various microchannel geometries on the overall heat transfer characteristics of the array has not been previously addressed. In this paper, different microchannel cross-sections are considered and the configuration of microchannels in an array is investigated. Considering the crucial requirement for sharp corners, in case of using capillary pressure difference as the driving force, a geometric optimization for different configurations in an array of microchannels is conducted. Dimensionless design charts, based on parametric models of various microchannel configurations, can then be utilized in the geometric design of an array of microchannels under different working conditions. Therefore, independently from the problem configuration, an optimized geometry of microchannels for any thermal application can be selected from the design charts. This work will assist the microchannel manufacturing process based on the robotic deposition of the fugitive organic ink impregnated with an epoxy resin [13].

2. Microchannel modelling

To capture the intricate flow and heat transfer phenomena within a microchannel having a large aspect ratio (on the order of 1000), a compromise between cross-sectional nodal resolution and computational time must be found [27]. The microchannel modelling considers the channels as a homogeneous material in order to investigate the effect of channel configuration on the thermal performance of the entire microfluidic chip. However particularly, for microfluidic chips without micropump, the absence of sharp edges for circular cross-sections significantly reduces the capillary pressure gradient necessary to provide flow inside the microchannels. Consequently, the modelling proposed here focuses only on triangular, rectangular, and trapezoidal cross-section geometries.

2.1 Single microchannel

Thermal microfluidic chips operate under different boundary conditions depending on the application in which the microchannels are used. The high aspect ratio of microchannels as well as their high effective conductivity causes a dominant one-dimensional heat flux along the microchannel. In the cases where the boundary heat flux is perpendicular to the microchannel axial direction, the heat flux turns to be in the axial direction in a reorientation zone between the evaporator/condenser and the adiabatic sections. The investigations of the characteristics of this zone (e.g. the length, heat flux in different directions, etc.) will allow the simplification of the boundary conditions. For example, if the reorientation zone is ignored, all heat fluxes applied to the microchannel can be assumed to be in the microchannel axial direction.

To consider the heat flux reorientation zone in a microchannel, a numerical model of a single microchannel is defined in ANSYS 10.0. The microchannel was modeled as a homogeneous material with equivalent material properties obtained from the literature [30]. It was demonstrated that the microchannel working fluid content had an effect on the thermal performance. An optimum content of 20–25% gave the best results [6]. Therefore, a fluid content of 22.5% by volume was used to derive the microchannel equivalent material properties. Table 1 lists the material properties used in the simulations for the microchannel. Fig. 1 shows a schematic configuration of the finite element model. Low conductivity of epoxy causes low heat transfer trough the adiabatic and the bottom surface in evaporator and condenser sections. The microchannel was meshed with 24000 elements and the model boundary conditions were applied according to Fig. 1. The heat fluxes at the

Table 1. Material properties for the epoxy and the microchannels.

Property	Epoxy	Microchannel*
Density (kg/m^3)	1500	225
Specific heat ($J/kg°C$)	940	2500
Thermal conductivity ($W/m°C$)	1	400
Thermal expansion ($°C^{-1}$)	30×10^{-6}	—
Young's modulus (GPa)	4	—
Poisson's ratio	0.35	—

* Effective properties based on a fluid content of 22.5% by volume.

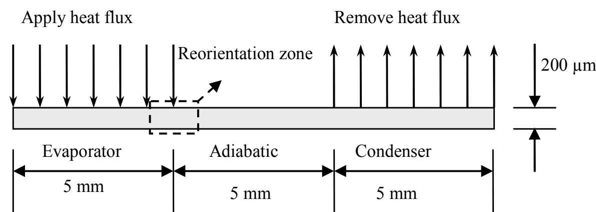

Fig. 1. Model of a single microchannel.

evaporator and the condenser sections were 15500 W/m^2 and -15500 W/m^2, respectively. The applied boundary conditions were selected in accordance with the typical working conditions in which microchannels operate.

Investigation of the reorientation zone under steady state conditions determines the heat transfer phenomena in this region. Considering the microchannel width (i.e., 200 μm), it was found that the length of the reorientation zone was less than three times the microchannel width. Therefore, ignoring the reorientation region in a microfluidic chip, which has a length of a few centimeters, does not affect the overall thermal behavior of microfluidic chips. Fig. 2 shows the heat flux in the steady state conditions for the x (axial) and y (transverse) directions for different positions along the width of the microchannel. The dimensionless length of the microchannel is obtained by dividing the axial position to the length of the channel. According to Fig. 1, the length of microchannel was divided into three equal sections: evaporator, adiabatic, and condenser sections. The adiabatic section of the microchannel, indicated in Fig. 2, has a uniform heat flux far from the reorientation zone. As shown in Fig. 2(a), the top line of the microchannel follows the applied boundary conditions, and there is a sudden peak in the beginning of adiabatic section. In the adiabatic section, the heat flux in the x-direction smoothly reaches the nominal value, towards the bottom line of the microchannel. A comparison between the value of the singularity peak at the reorientation zone with adiabatic section and the nominal value of heat flux in the x-direction is shown in Fig. 2(a).

Similarly, Fig. 2(b) shows the y-direction heat flux in different positions of the microchannel. The singularity peak value at the reorientation zone decreases towards the bottom line of the microchannel. A comparison between the reorientation peaks and the nominal value of y-direction heat flux is also

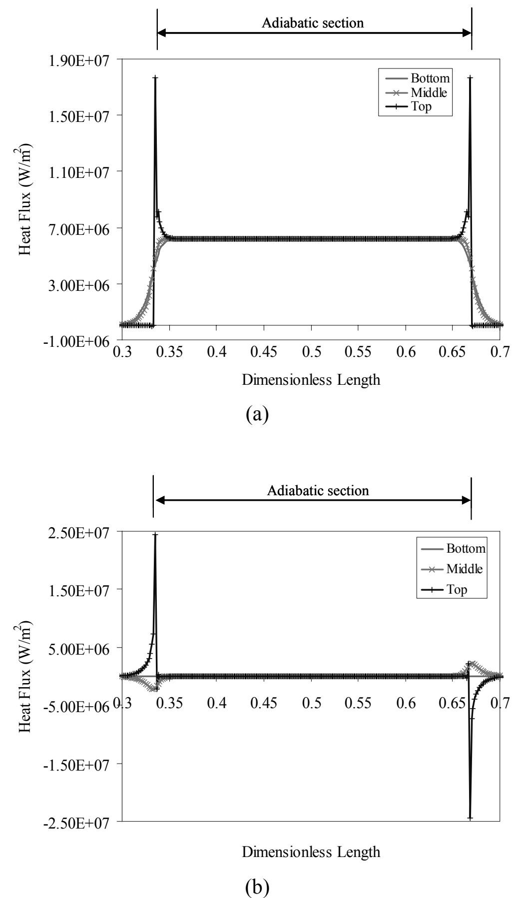

Fig. 2. Heat flux for bottom, top, and middle of the microchannel: a) x-direction b) y-direction.

shown in Fig. 2(b).

The results of Fig. 2 suggest that outside the reorientation region, the direction of applied heat flux (i.e., boundary conditions) has no effect on the overall thermal performance of microfluidic chip. Thus, regardless of the applications of microfluidic chip, the heat flux boundary conditions can be applied in the axial direction of microchannels and that will cause small errors only in the reorientation zone.

2.2 Array of microchannels

The heat transfer process of an array of microchannels was modeled using ANSYS Workbench 10.0 finite element software. Similar to the model of a single microchannel, the microchannels were modeled as homogeneous materials with equivalent material, and standard epoxy properties were used for the microchannels surrounding material. The material properties of microchannels and epoxy are listed in Table 1. A parametric model was developed to investigate the effect of geometry on the thermal behavior of an array of five microchannels. The parametric model provides the ability to change the geometry and boundary conditions in the adiabatic section and to obtain the optimum configuration. Fig. 3(a) shows the

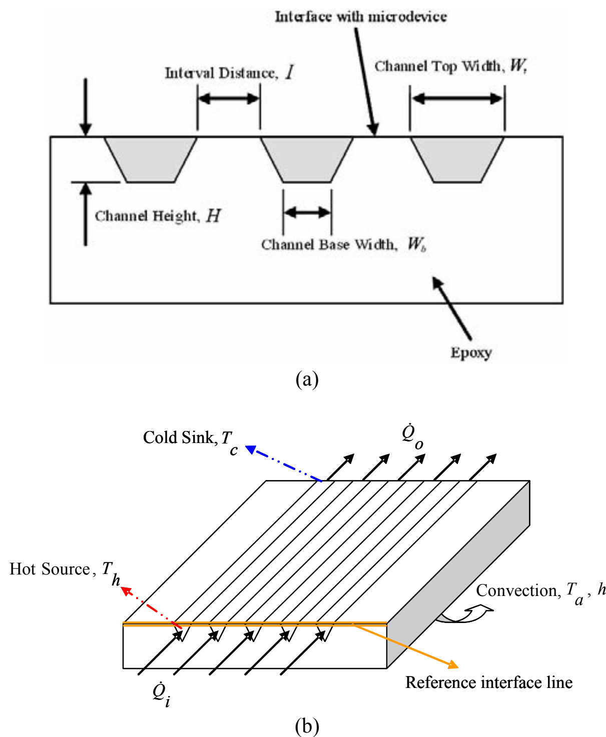

Fig. 3. (a) Geometric parameters used in the parametric model; (b) Typical boundary conditions applied to the adiabatic section of microchannels array.

geometric parameters used in the parametric model. The adiabatic section was meshed with 12500 elements and the model boundary conditions were applied according to Fig. 3(b). The hot source (T_h) and cold sink (T_c) temperatures were 90 *°C* and 10 *°C* respectively, while the ambient temperature (T_a) was set to 40 *°C*. Similar to the single microchannel modelling the heat fluxes at the hot source ($\dot{Q}_i$) and at the cold sink ($\dot{Q}_o$) were 15500 W/m^2 and -15500 W/m^2 respectively. The convection heat transfer coefficient (h) was set to 200 W/m^2K. As shown in the single microchannel modelling, in the analysis of the adiabatic section, the heat flux can be assumed to be in the microchannel axial direction.

Simulations were conducted for steady state and transient conditions. For the transient analysis, the heat fluxes and hot source temperature were ramped to their steady state values in 5 *s*. Constant conditions were maintained for 20 *s* before they were ramped down to the steady state in 5 seconds. With an initial temperature of 22 *ºC* for the microfluidic chip and 10 *ºC* for the heat sink, a fast ramp rate for the heat fluxes and the hot source temperature was simulated.

2.2.1 Steady state results

The efficiency of the microchannels array was investigated from the steady state temperature distribution at the interface between the microchannels and the other parts of the integrated system, like a microelectronic device (Fig. 3(a)). Since controlling the temperature and the heat flux in the microdevices are the main objectives of thermal microfluidic chips, the effect of different geometric parameters on the interface temperature distribution is of particular interest. Given that the microchannels were modeled as a high conductive material, in the hot source area, the microchannel temperature was higher than the temperature in the surrounding epoxy. Similarly, in the cold sink region, the microchannel temperature was lower than that of the surrounding epoxy, and that caused important temperature gradients. In the following analysis, the beginning of the adiabatic section, shown by the reference interface line in Fig. 3(b), is analyzed.

In the thermal model, the temperature along the reference interface line was classified according to three ranges: $0.83T_h < T < 0.89T_h$, $0.89T_h < T < 0.94T_h$ and $0.94T_h < T < T_h$. Fig. 4(a) presents the variation of the steady state interface temperature distribution with the dimensionless microchannel interval distance (I/W_t , see Fig. 3(a)). The simulations were conducted for a triangular microchannel cross-section with H = 400 μm, W_t = 400 μm and W_b = 0. The percentage reported on Fig. 4(a) represents the length of each of these temperature ranges over the total length of reference interface line in a given cross-section. A dimensionless average temperature (T_{avg}), which is normalized by dividing by the hot source temperature (T_h), at the interface is also presented. The results showed that for short microchannel spacing, $I/W_t < 1$, the interface temperature was very close to the hot source temperature. For I/W_t = 1–2, the interface temperature distribution became less uniform. For $I/W_t > 2$, significant interface nonuniformity was observed with an increase of the percentage of interface temperature between $0.83T_h < T < 0.89T_h$. Since the amount of heat transfer in a given cross-section is dependent on the number of channels located in that area, for heat removal applications the maximum possible channels which meet the requirements of interface temperature should be chosen. According to the results of Fig. 4(a), for heat removal applications, a value of I/W_t = 2 is recommended to have a compromise between the amount of heat transfer and the interface temperature. However, for different applications with various required temperature, the I/W_t ratio can be selected from Fig. 4(a).

Fig. 4(b) presents the variation of the steady state interface temperature distribution with the dimensionless microchannel width (W_b/W_t, see Fig. 3(a)). The effect of choosing a triangular cross-section (W_b/W_t = 0) was considered in Fig. 4(a), and in Fig. 4(b) a trapezoidal cross-section ($W_b/W_t > 0$) was investigated. The simulations were conducted with the following constant parameters: H = 200 μm, W_t = 400 μm and I = 1500 μm (I/W_t = 3.5). The surface temperatures were classified according to the same procedure described previously and the average temperature of the interface was determined. The results showed that for a narrow microchannel base width, $W_b/W_t < 0.5$, the interface temperature was not very uniform. This result was consistent with the previous analysis for a triangular cross-section with I/W_t = 3.5 as the trapezoidal cross-section behaves similarly to a triangular cross-section at

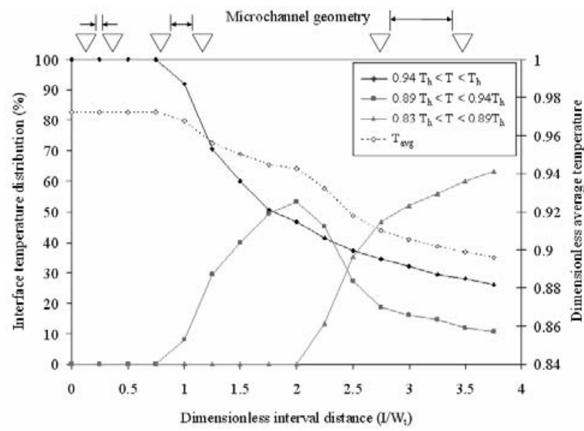

(a)

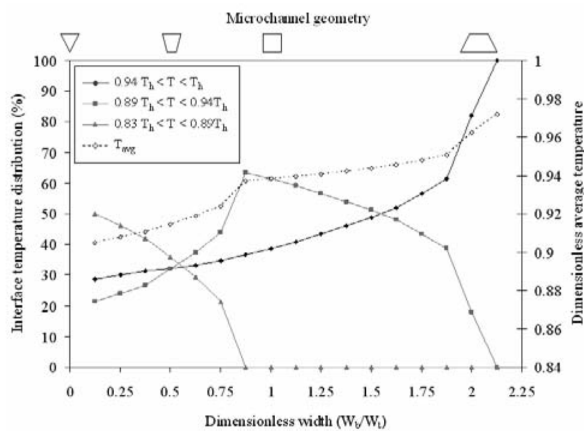

(b)

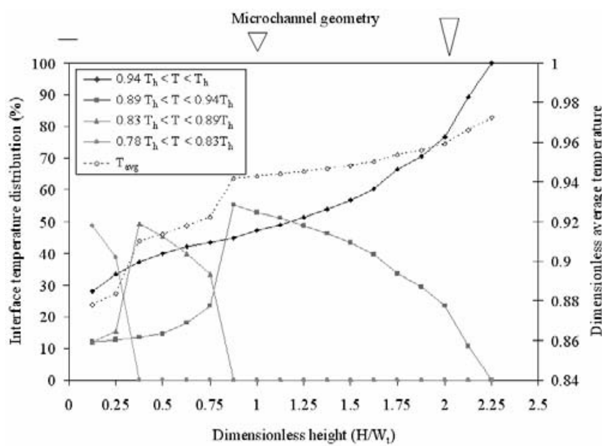

(c)

Fig. 4. (a) Effect of dimensionless interval distance (I/W_t) on the interface temperature distribution, $H = 400\ \mu m$, $W_t = 400\ \mu m$ and $W_b = 0$; (b) Effect of dimensionless width (W_b/W_t) on the interface temperature distribution, $H = 200\ \mu m$, $W_t = 400\ \mu m$ and $I = 1500\ \mu m$; (c) Effect of dimensionless height (H/W_t) on the interface temperature distribution, $I = 800\ \mu m$, $W_t = 400\ \mu m$ and $W_b = 0\ \mu m$. The corresponding microchannel geometry is shown at the top of each design chart.

small values of W_b/W_t. For $W_b/W_t > 0.875$ the interface temperature distribution became more uniform and at $W_b/W_t = 2.125$ the maximum interface temperature was achieved. As it can be seen in Fig. 4(b), for $W_b/W_t > 2.125$ the interface temperature was entirely in the range of $0.94T_h < T < T_h$ and increasing W_b/W_t did not have any effect. According to Fig. 4(b), the slope for the $0.94T_h < T < T_h$ range was more or less constant up to $W_b/W_t = 1.5$. For $W_b/W_t > 1.5$, a rapid change of the interface temperature was noticeable. This result was confirmed by the variation of the average interface temperature. As a result, Fig. 4(b) can be used as a design chart to select the optimized configuration of microchannels for different applications. Particularly, for heat removal applications, a value of $W_b/W_t = 1.5$ is recommended for a maximum heat transfer coefficient and a dimensionless average temperature of 0.944 in the interface.

Fig. 4(c) presents the variation of the steady state interface temperature distribution with the dimensionless microchannel height (H/W_t see Fig. 3(a)). The simulations were conducted for a triangular microchannel cross-section with $I = 800\ \mu m$, $W_t = 400\ \mu m$ and $W_b = 0\ \mu m$. For a very small dimensionless height ($H/W_t < 0.25$) the triangular microchannel geometry was very close to a line, because the height was very small compared to the microchannel width. In this case the hot spots ($T \approx T_h$) on the interface temperature were just located at the channels' top surfaces, almost 30% of the total interface. Considering the $0.94T_h < T < T_h$ data, the curvature slope decreases as H/W_t approaches 0.875 and increases for $H/W_t > 0.875$. This behavior indicated that the heating rate at the interface was high, thus small increases in the H/W_t ratio led to a rapid increase of the interface temperature. The average temperature interface also showed the same trend as observed on Fig. 4(c). Similar to Fig. 4(a) and 4(b), Fig. 4(c) can be used as a design chart in different applications of microfluidic chips. For thermal removal applications, $H/W_t = 0.875$ satisfied both a minimum interface temperature and a maximum heat transfer. It has to be mentioned that $H/W_t = 0.875$ corresponds to an equilateral triangle; therefore, for triangular microchannels serving in the heat removal application, the best performance was achieved with an equilateral triangle.

The presented design charts (Fig. 4) can be utilized to design microfluidic chips operating in different applications. As an example, the design of a microfluidic chip for polymerase chain reaction (PCR) for DNA amplification is presented. The PCR amplification process contains three sectors with different process temperatures: denaturation, annealing, and extension. The annealing sector, which contains the attachment of separated single strand DNA to a specific primer, takes place at 54 ºC [31]. Subsequently, the design process for appropriate microfluidic chip in this application is presented. In this application, the temperature uniformity at the interface has a higher design priority compared to the amount of heat transferred in the microfluidic chip. Fig. 4(c) shows that the dimensionless average temperature is very sensitive to microchannel height, especially for $H/W_t < 0.875$. Therefore, to consider the possi-

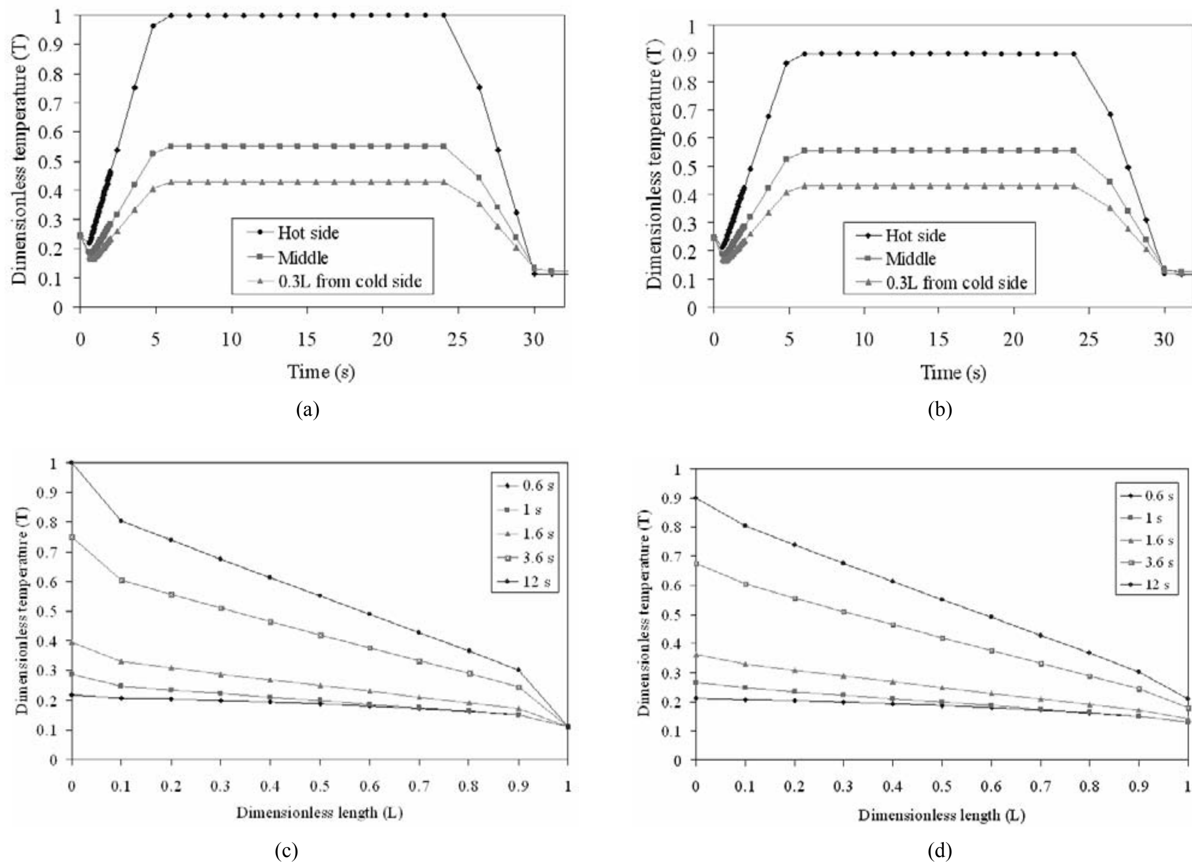

Fig. 5. Transient response of microfluidic chip in different positions of top surface for (a) microfluidic chip microchannel and (b) surrounding epoxy. Interface temperature gradient along the microfluidic chip length at different time for (c) microfluidic chip microchannel and (d) surrounding epoxy.

ble difficulties in the manufacturing of microfluidic chip, use of trapezoidal channel is recommended. Fig. 4(b) shows less sensitivity of dimensionless average temperature to the dimensionless width for W_b/W_t > 0.875. Thus, W_b/W_t = 1.5 is suggested to have a dimensionless average temperature between 0.94 and 0.95. In this case, the microchannel specifications are: I = 1500 μm, W_t = 400 μm, H = 200 μm, and W_b = 600 μm. Applying a T_h = 57 ºC causes an average temperature of 54 ºC with a maximum tolerance of 6% in the entire interface.

2.2.2 Transient results

The results of the transient heat transfer analysis of the top surface temperature are presented in Fig. 5. In this study the microfluidic chip was assumed to be made out of homogeneous materials. In this case, the results presented in Fig. 5(a) and Fig. 5(b) suggest that the microfluidic chip had a very fast response time as steady state conditions were almost instantaneously achieved in both the microchannel and the surrounding epoxy. In the worst conditions, a maximum response time of much less than 2 *s* was necessary to reach the steady state conditions. This fact proves that microfluidic chips are ideal for temperature sensors.

The evolution of the temperature gradient along the microfluidic chip length with time is presented in Fig. 5(c) and Fig. 5(d). Aside from the regions close to the heat source and the cold sink, the temperature profiles were linear. As observed in the steady state analysis, there was a small temperature difference between the microchannel and the surrounding epoxy. The fast convergence of the transient response to the steady state condition indicated that the results of Fig. 5(c) and Fig. 5(d) correspond to the steady state responses under different boundary conditions of hot source temperature. For example, a transient response after 3.6 *s* in the microchannel can be interpreted as a steady state response with a hot source temperature of 74 percent of the original hot temperature.

3. Conclusions

In this work the effect of the microchannels configuration on the heat transfer efficiency of microfluidic chip was investigated. General investigation on different boundary conditions was carried out and the results suggested that disregarding the small reorientation section, the heat flux boundary conditions can always be assumed to be in the microchannel axial direction.

Knowing the limited applications of circular cross-section, in the current research, triangular, rectangular and trapezoidal microchannels were investigated. The effect of different geometric parameters on the interface temperature of microfluidic chip was investigated and geometric design charts were presented. The geometric design charts can be used to design the geometry of various microfluidic chips functioning under different situations. According to the presented design charts for a thermal removal microfluidic chips, as a practical application, an interval distance of twice the width for triangular microchannels was recommended for optimum performances. For triangular channels, a compromise between the maximum heat transfer and minimum interface temperature was achieved at a height to the width ratio of 0.875, which corresponds to equilateral triangles. For trapezoidal microchannels, a base to top width ratio of 1.5 was recommended. As another example of using design charts, a microfluidic chip for the annealing sector of a Polymerase Chain Reaction (PCR) for DNA amplification was designed.

Finally, the transient behavior of microfluidic chips under a high rate ramp demonstrated a required time of much less than 2 *s* in the worst conditions to reach steady state conditions. Thus, steady state behavior of the system under different boundary temperatures can be simulated by a single transient response that presents the instant in which the boundary temperature is equal to the desired temperature. Low response time of microfluidic chips makes them ideal form temperature sensing applications.

Acknowledgment

The authors acknowledge the funding from the Natural Sciences and Engineering Research Council of Canada Strategic Grant Program, McGill Max Stern Scholarship and McGill Graduate Students Fellowship. We would like to thank David de Koninck and Ronald Lawand from the Composite Materials and Structures Laboratory at McGill University for their assistance.

References

[1] T. P. Cotter, Principles and prospects for micro heat pipes, *5th International Heat Pipe Conference*, Tsukuba, Japan (1984) 328-335.

[2] P. Sabounchi, et al., Soft-state biomicrofluidic pulse generator for single cell analysis, *Applied Physics Letters*, 88 (18) (2006) 183901.

[3] A. Hiratsuka, et al., Organic plasma process for simple and substrate-independent surface modification of polymeric BioMEMS devices, *Biosensors and Bioelectronics*, 19 (12) (2004) 1667-1672.

[4] A. Faghri, *Heat pipe science and technology*, Taylor & Francis, Washington, DC (1995).

[5] C. W. Liu, C. Gau and B. T. Dai, Design and fabrication development of a micro flow heated channel with measurements of the inside micro-scale flow and heat transfer process, *Biosensors and Bioelectronics*, 20 (1) (2004) 91-101.

[6] S. Launay, V. Sartre and M. Lallemand, Experimental study on silicon micro-heat pipe arrays, *Applied Thermal Engineering*, 24 (2-3) (2004) 233-243.

[7] L. J. Brognaux, et al., Single-phase heat transfer in micro-fin tubes, *International Journal of Heat and Mass Transfer*, 40 (18) (1997) 4345-4357.

[8] J. Li, G. P. Peterson and P. Cheng, Three-dimensional analysis of heat transfer in a micro-heat sink with single phase flow, *International Journal of Heat and Mass Transfer*, 47 (19-20) (2004) 4215-4231.

[9] M. Ghajar, J. Darabi and N. Crews Jr, A hybrid CFD-mathematical model for simulation of a MEMS loop heat pipe for electronics cooling applications, *Journal of Micromechanics and Microengineering*, 15 (2) (2005) 313-321.

[10] S.-W. Kang, S.-H. Tsai and M.-H. Ko, Metallic micro heat pipe heat spreader fabrication, *Applied Thermal Engineering*, 24 (2-3) (2004) 299-309.

[11] C. H. Shen and C. Gau, Thermal chip fabrication with arrays of sensors and heaters for micro-scale impingement cooling heat transfer analysis and measurements, *Biosensors and Bioelectronics*, 20 (1) (2004) 103-114.

[12] D. M. Leatzow, et al., Attachment of plastic fluidic components to glass sensing surfaces, *Biosensors and Bioelectronics*, 17 (1-2) (2002) 105-110.

[13] D. Therriault, S. R. White and J. A. Lewis, Chaotic mixing in three-dimensional microvascular networks fabricated by direct-write assembly, *Nature Materials*, 2 (4) (2003) 265-271.

[14] T. Kimura, et al., Thermal conductivity and RF signal transmission properties of Ag-filled epoxy resin, New Orleans LA, United States, (2003) 1383-1390.

[15] J. F. Mark, et al., Array Biosensor: Optical and Fluidics Systems, *Biomedical Microdevices*, V1 (2) (1999) 139-153.

[16] B. Suman and N. Hoda, Effect of variations in thermophysical properties and design parameters on the performance of a V-shaped micro grooved heat pipe, *International Journal of Heat and Mass Transfer*, 48 (10) (2005) 2090-2101.

[17] B. Suman, S. De and S. DasGupta, A model of the capillary limit of a micro heat pipe and prediction of the dry-out length, *International Journal of Heat and Fluid Flow*, 26 (3) (2005) 495-505.

[18] H. B. Ma and G. P. Peterson, Experimental investigation of the maximum heat transport in triangular grooves, *Transactions of the ASME. Journal of Heat Transfer*, 118 (3) (1996) 740-746.

[19] G. P. Peterson, A. B. Duncan and M. H. Weichold, Experimental investigation of micro heat pipes fabricated in silicon wafers, *Journal of Heat Transfer, Transactions ASME*, 115 (3) (1993) 751-756.

[20] J. T. Dickey and T. T. Lam, Impact of channel geometry on heat transfer in microchannel for high density electronics cooling, Kauai, Hi, United States (2001) 681-686.

[21] J. Li and G. P. Peterson, Geometric optimization of a micro heat sink with liquid flow, *IEEE Transactions on Components and Packaging Technologies*, 29 (1) (2006) 145-154.

[22] P. M. Y. Chung, et al., Two-Phase Flow Through Square and Circular Microchannels-Effects of Channel Geometry, *Journal of Fluids Engineering*, 126 (4) (2004) 546-552.

[23] L. Zhang, et al., Phase change phenomena in silicon microchannels, *International Journal of Heat and Mass Transfer*, 48 (8) (2005) 1572-1582.

[24] H. B. Ma and G. P. Peterson, Temperature variation and heat transfer in triangular grooves with an evaporating film, *Journal of Thermophysics and Heat Transfer*, 11 (1) (1997) 90-97.

[25] P. C. Stephan and C. A. Busse, Analysis of the heat transfer coefficient of grooved heat pipe evaporator walls, *International Journal of Heat and Mass Transfer*, 35 (2) (1992) 383-391.

[26] B. Suman and P. Kumar, An analytical model for fluid flow and heat transfer in a micro-heat pipe of polygonal shape, *International Journal of Heat and Mass Transfer*, 48 (21-22) (2005) 4498-4509.

[27] M. Rahmat, Geometric optimization for a thermal microfluidic chip, in *Mechanical Engineering*. 2007, McGill University: Montreal. 124.

[28] I. Tiselj, et al., Effect of axial conduction on the heat transfer in micro-channels, *International Journal of Heat and Mass Transfer*, 47 (12-13) (2004) 2551-2565.

[29] T. Motoyama and R. Hackam, Effect of temperature and water salinity on hydrophobicity of epoxy resin, Kitchener, ON (2001) 157-160.

[30] Y. A. Cengel, *Heat Transfer: a practical approach*, Second ed, McGraw-Hill, New York (2003).

[31] N.-C. Tsai and C.-Y. Sue, SU-8 based continuous-flow RT-PCR bio-chips under high-precision temperature control, *Biosensors and Bioelectronics*, 22 (2) (2006) 313-317.

Meysam Rahmat Received his B.Sc. in Mechanical Engineering from Iran University of Science and Technology (IUST) in 2004. He completed his Master of Engineering in the department of Mechanical Engineering at McGill University, and started his Ph.D. in the same department in 2007.

Pascal Hubert (Ph.D. Metals and Materials Engineering, The University of British Columbia) holds a Canada Research Chair in Advanced Composite Materials. He is an associate professor at McGill University in the Department of Mechanical Engineering (since Septem-ber 2002). Dr. Hubert has 90 refereed journal and conference publications with over 20 publications in the area of nanocomposites and on the processing and performance of composite materials.